Neurotoxicology 93 (2022) 152–162

Contents lists available at ScienceDirect

Neurotoxicology

journal homepage: www.elsevier.com/locate/neuro

Chlorpyrifos, permethrin and cyfluthrin effect on cell survival, permeability, and tight junction in an in-vitro model of the human blood-brain barrier (BBB)

Deepika Deepika [a,1], Saurav Kumar [a,1], Natalia Bravo [b], Roser Esplugas [a,c], Marco Capodiferro [b], Raju Prasad Sharma [a], Marta Schuhmacher [a], Joan O. Grimalt [b], Jordi Blanco [c], Vikas Kumar [d,*]

[a] Environmental Engineering Laboratory, Departament d'Enginyeria Quimica, Universitat Rovira i Virgili, Av. Països Catalans 26, 43007 Tarragona, Catalonia, Spain
[b] Institute of Environmental Assessment and Water Research (IDAEA) - Spanish Council for Scientific Research (CSIC), Department of Environmental Chemistry, Jordi Girona, 18, 08034 Barcelona, Catalonia, Spain
[c] Laboratory of Toxicology and Environmental Health, School of Medicine, IISPV, Universitat Rovira i Virgili, Reus, Spain
[d] IISPV, Hospital Universitari Sant Joan de Reus, Universitat Rovira I Virgili, Reus, Spain

ARTICLE INFO

Edited by Dr. T.J. Shafer

Keywords:
Blood-brain-barrier
HCMEC/D3
Chlorpyrifos
Insecticides
Pyrethroids
Permethrin
Cyfluthrin
Permeability
Efflux ratio

ABSTRACT

The blood-brain barrier (BBB) is a structural and functional interface between the plasma and the human brain. Predictive BBB in-vitro models like immortalized human capillary microvascular endothelial cells (HCMEC/D3) can be used to explore the BBB disruption potential of daily exposed chemicals. The present study was focused on investigating the human BBB permeation potential of one organophosphate pesticide, chlorpyrifos (CPF), and two pyrethroids, permethrin (PMT) and cyfluthrin (CFT). HCMEC/D3 cells were exposed to the chemical and the time-dependent pass across BBB along with permeation coefficient (Papp) was calculated. Transendothelial electrical resistance (TEER) was measured for the cells to check the monolayer formation and later to check the reduction in integrity after chemical exposure. Real time PCR was conducted to investigate the effect of chemicals on the expression BBB's tight and adherens junction proteins. Calculated Papp value for three chemicals was in the following order: CPF>CFT>PMT, where CPF showed the highest permeation coefficient. TEER calculation showed that the integrity decreased after CPF exposure which was in concordance with Papp value whereas for other chemicals, no change in TEER after exposure was observed. In addition, the transwell study showed a higher efflux ratio (ER) (>2) of CFT indicating that CFT could be a substrate for active transport. For CPF and PMT, ER was less than 2, so no active transport seems to be involved. The evaluation of the mRNA expression analysis revealed a statistically significant decrease in Occludin (OCLN) gene expression for CPF, VE-Cadherin (CDH5) for PMT and Zonula Occludens (ZO1) expression for CFT. Our study showed that CPF has the highest potential for inducing cell death, higher permeation, and capability to induce BBB dysfunction than among the above-mentioned chemicals. Additionally, the results of the permeation study could be useful to build a human PBPK model using in vitro-to-in vivo extrapolation approach.

1. Introduction

Chlorpyrifos (CPF) is a widely used organophosphate pesticide (OP) for pest control in animals, plants for agriculture and public health applications (Li and Ehrich, 2013; Goel et al., 2005). Several epidemiological studies revealed that the general population might be getting exposed to CPF through air, food, soil and water (Eaton et al., 2008; Oliver et al., 2000). Over time, studies have focused on the neurotoxic effects of CPF. For instance, CPF has been associated with neurodevelopmental disorders in infants and children (Guo et al., 2019). Further, it has been shown that CPF inhibits brain cholinesterase, a target neurotransmitter associated with behavioral disturbances in exposed rodents (Saunders et al., 2012; Whitney et al., 1995). CPF has recently been banned for sale in Europe due to geno- and neurotoxicity but its use continues in many developing nations (EU-Wide, n.d.). In recent years, CPF has been replaced by pyrethroids like permethrin

* Corresponding author.
E-mail address: Vikas.kumar@urv.cat (V. Kumar).
[1] Both authors are contributed equally to this work.

https://doi.org/10.1016/j.neuro.2022.09.010
Received 17 June 2022; Received in revised form 14 September 2022; Accepted 23 September 2022
Available online 24 September 2022

(PMT) and cyfluthrin (CFT) (Fluegge et al., 2016; Rodríguez et al., 2018). Exposure to these insecticides may occur through dietary intake, respiratory uptake and dermal contact (Rodríguez et al., 2018). These insecticides have also shown neurotoxic effects; however, their mechanism and potency might differ based on the exposure. For instance, in a comparative study for neurotoxicity, it was observed that both pyrethroids (PMT and CFT) had different effects on sodium, chloride and calcium ion channels in the brain (Breckenridge et al., 2009). Type I pyrethroid like PMT mainly changes the conformation of sodium channel, whereas type II pyrethroid like CFT act on chloride channel including GABA receptors (γ-aminobutyric acid) (López-Aceves et al., 2021). However, CPF mainly acts by inducing cholinergic crisis in human due to irreversible inhibition of cholinesterase, an enzyme that hydrolyse acetylcholine (ACh) (Burke et al., 2017). Similarly, the dose at which neurotoxicity is observed varies for the insecticides indicating that they might have the ability to cross the human blood-brain-barrier (BBB) at specific exposure levels.

The BBB is a network of complex tight junctions formed by specialized capillary endothelial cells lining the brain microvessels whereas neighbouring cells like astrocytes and pericytes forms the neurovascular unit. However, the major interface is formed by endothelial cells preventing the transport of toxic compounds from blood to the cerebrospinal fluid (CSF) or nervous system (Abbott, 2013). Transport of hydrophilic compounds across the BBB is restricted, however lipophilic or uncharged compounds can pass by passive diffusion. Nevertheless, the efflux transporters like P-GP (P glycoprotein) and BCRP (Breast cancer resistant protein) often regulate the movement of lipophilic compounds (Abbott, 2013). Numerous in-vitro models of human BBB based on endothelial cells like human brain microvascular endothelial cells (HBMEC) and human pluripotent stem cells (hPSC) have been developed for studying the transport of xenobiotics. Non-endothelial cell lines like Caco-2, MDCK (Madin-Darby Canine Kidney), and LLC-PK1 (Pig Kidney Epithelial cells) are also used as a model for studying permeation, but they cannot replicate the complexity of human BBB (Gericke et al., 2020). Immortalized Human Microvascular Endothelial Cell lines (HCMEC/D3) are the extensively used in-vitro model to study the chemical kinetics and gene expression at the BBB. They form the tight junction (Weksler et al., 2013a) and serve as a suitable model for studying the transport kinetics of xenobiotics.

We did not find any in-vitro study in the literature related to permeation potential for CFT and PMT. However, there are some studies in rats with PMT and CFT exposure showing BBB disruption, but most studies focused on biomarkers altered in the brain rather than concentration detected after a particular exposure (Singh et al., 2009; Rodríguez et al., 2016; Syed et al., 2016; Abu-Qare and Abou-Donia, 2003; Abdel-Rahman et al., 2004). For CPF, one study was published in literature with RBE4 cell lines where permeation was calculated but with rat cell lines. Currently there are limited quantitative permeation studies for these chemicals suggesting a data gap for understanding BBB toxicokinetics.

As per literature, most xenobiotics that enter the brain are less than 500 Da, neutral and lipophilic which can diffuse through brain endothelial cells (Brian Houston and Carlile, 1997). However, many xenobiotics still do not follow this rule. Conducting animal experiments for thousands of chemicals is time-consuming, so in-vitro models can be considered one of the alternatives for permeability study. There are some BBB differences in animals and humans at the molecular level, i.e. enzymes and protein expression at the tight junction, which can alter the BBB permeability (Wilhelm and Krizbai, 2014). For example, a study comparing rat and human BBB showed more than two-fold difference with P-GP, MDRP4 (multidrug resistance-associated protein 4), OAT3 (organic anion transporter 3) and L1 type amine acid (Hoshi et al., 2013). In the same study, more than a two-fold difference in CLDN-5 expression was shown in humans compared to rats, monkeys and marmosets in the in-vivo study (Hoshi et al., 2013). Since CLDN-5 is one of the major genes expressed at BBB and plays a pivotal role in the tight junction regulation, human cell lines should be used for studies related to permeation potential. Regulatory bodies like FDA (Food and Drug Administration) recommends the need to conduct test for P-GP for the new molecular entities (NME) to understand the pharmacokinetics within the central nervous system (CNS) and drug-drug interaction at an early stage of drug discovery (Akamine et al., 2019). Such kind of in-vitro tests can be used for these assays to reduce the dependence on animal models. In the case of environmental chemicals, test like P-GP assay and transwell permeability can be conducted as initial tests to classify chemicals as CNS+ or CNS- before evaluating their neurotoxic potential using in-vitro cell lines.

This study aimed to investigate the toxicokinetics of CPF, PMT and CFT in an HCMEC/D3 model of the human BBB. Initially, cell viability was measured to evaluate cytotoxicity of the chemical. Further, transendothelial electrical resistance (TEER) was calculated to confirm the tight junction formation. Later, a bidirectional permeability experiment was conducted using a transwell assay to calculate the permeation profile. In-vitro results were correlated with in-vivo permeability using IVIVC (in-vitro to in-vivo correlation). Changes in mRNA (or gene) expression of several tight junctions were also evaluated by RT-qPCR. In future, characterization of toxicokinetic properties of these chemicals could provide a basis to develop brain-physiologically based pharmacokinetic model (PBPK) using in-vitro data and decrease the uncertainty in humans risk assessment.

2. Material and methodology

2.1. Materials

Chlorpyrifos (CPF), permethrin (PMT) and cyfluthrin (CFT) were purchased with purity of 98.0 % CPF, 90.0 % sum of cis+trans PMT and 95 % (sum of diastereomers) from Sigma Aldrich (St. Louis, MO, USA). Immortalized human brain microvascular endothelial cell lines (HCMEC/D3) were obtained from Cederlane labs (Burlington, Canada). Endothelial cell growth medium (EGM) along with supplements was purchased from Sigma Aldrich (St. Louis, MO, USA). MTT (3-(4,5-dimethylthiazol-2-yl)− 2,5-diphenyltetrazolium bromide) reagent, trypan-blue, trypsin-EDTA (ethylenediaminetetraacetic acid), HBSS (Hanks Balanced Salt Solution), HEPES (4-(2-hydroxyethyl)− 1-piperazineethanesulfonic acid), DMSO (dimethyl sulfoxide) and rat tail collagen type 1 were purchased from Sigma Aldrich (St. Louis, MO, USA). Transwell inserts (6-well and 12-well) were obtained from Sigma Aldrich and Corning (St. Louis, MO, USA).

2.2. Cell growth and exposure

HCMEC/D3 cell lines were cultured in endothelial cell growth medium (2 % v/v) supplemented with fetal calf serum (0.02 ml/ml), endothelial cell growth supplement (0.004 ml/l), epidermal growth factor (0.1 ng/ml), basic fibroblast growth factor (1 ng/ml), heparin (90 μgm) and hydrocortisone (1 μgm/ml) at 37 °C, 5 % CO2 and 95 % relative humidity. For ensuring BBB properties, the passage used ranged from 27 to 34 (Weksler et al., 2013b). Cells were grown to 80–90 % confluency for 3–5 days on a T75 flask with a change of medium every 2–3 days. Then trypsin-EDTA was used as a dissociation buffer and cells were resuspended in EGM. Resuspended cells were counted and used for sub-culturing for further experiments. For all the experiments, cells were seeded at the density of 3–5 * 10^4 cells/cm^2.

2.3. Cell Viability assay

Cells were cultured in 48 well plates and incubated at different concentrations for three chemicals along with DMSO (0.1 % vehicle) treatment. Cells were treated with different concentrations of CPF (0, 1, 5, 10, 15, 30 and 60 μM), PMT (0, 1, 50, 100, 200, 600, and 800 μM), and CFT (0, 50, 100, 200, 600, and 800 μM) from low to high for 24 h. Cells

were cultured for 2–3 days before starting the treatment. Cell viability was measured at 24 h by adding 50 μl (5 mg/ml) MTT. They were kept for 4 h in an incubator for the formation of formazan and then DMSO was added to dissolve the formazan. Absorbance was measured using a UV-Vis spectrophotometer at 560 nm. The viability test was carried out in triplicate. Cell viability was calculated as a percentage of absorbance compared to control (Eq.1).

$$Cell \quad Viability = \frac{Abs_{sample}}{Abs_{control}} * 100 \tag{1}$$

2.4. Bidirectional permeability assay and TEER measurement

For the permeability experiment, HCMEC/D3 cells were cultured on 12-well transwell inserts (0.4 μm pores, PET) with EGM medium (Fig. 1). Transwell inserts were coated with rat tail collagen type 1 diluted in 70 % ethanol and dried for minimum 3 h before seeding the cells. Cells were grown to confluence for a minimum 7–8 days with change in the medium after 2–3 days until a monolayer was formed. The TEER was measured on every second day of cell growth for 7–8 days on inserts using the Millicell ERS2 system for evaluating the tightness of the cell monolayers. Blank resistance was determined before starting the measurement and an electrode tip was kept in the disinfecting solution for 15 min followed by the cell culture medium (5–10 min) for equilibration. Cells were allowed to reach room temperature to avoid temperature changes affecting the resistance. The electrode was immersed so that a shorter tip was in the insert and a longer tip in the outer well. Precaution was taken so that the shorter tip did not touch the surface of cells. Inserts with collagen and without cells were considered as blank and all the measurements were done in duplicate. The TEER was calculated by the Eqs. (2) and (3), that is:

$$\text{Resistance}_{\text{cell monolayer}} = \text{Resistance}_{\text{cell}} - \text{Resistance}_{\text{blank}} \tag{2}$$

$$\text{Unit arearesistance}_{\text{cell monolayer}} = \text{Resistance} * \text{Effective membrane area}\left(\text{cm}^2\right) \tag{3}$$

All transwell assays were performed with transport buffer (Hanks balanced salt solution with 20 mM HEPES, 25 Mm D-glucose, 1.25 mM CaCl2, and 0.5 mM MgCl2) at pH 7.4. Before starting the experiment, both sides of the inserts were prewashed with transport buffer (approximately 15 min in an incubator) and then the medium was decanted. This procedure was repeated 2 times for complete removal of EGM. After washing, the inserts were transferred to a new plate before starting the experiment to avoid carryover of cell growth medium. Assays were performed in two concentrations (min and max) with stock solution diluted in transport buffer for all chemicals. Well plates were incubated at 37 °C on orbital shaker with moderate speed (100 rpm) to maintain sink conditions. Media samples (100–200 μl) were removed in determined time points: 30, 60, 120, 240 and 300 min from basolateral compartments to study the A-B transport; and from the apical compartment to study the B-A transport in two separate experiments. In a similar study to at 300 min, sample was withdrawn from apical compartment for A-B transport and basolateral compartment for B-A transport. Permeability test was carried out in triplicate. Samples were maintained at − 80ºC until analysis. At 300 min after chemical exposure, membrane integrity was again measured with TEER. Fig. 1

2.5. Sample analysis by GC-ECD

Collected media samples (200 μl) were placed into centrifuge tubes and pesticides were extracted by adding n-hexane. The supernatant n-hexane layer was aspirated and placed into a chromatographic vial, followed by reextraction two more times with n-hexane. All the n-hexane extracts were combined and reduced to dryness under a very gentle stream of nitrogen. Finally, they were dissolved with 200 μl of parathion-ethyl (internal standard) in isooctane.

Organophosphate pesticide and pyrethroid were quantified by gas chromatography with electron captor detection (GC-ECD, Agilent Technologies 7890 A). The instrument was equipped with an HP-5MS capillary column (60 m length, 0.25 mm internal diameter, 0.25 μm film thickness; JW Scientific) protected with a retention gap. Two microliters were injected in splitless mode. Injector and detector temperatures were 250 and 320 °C, respectively. The oven temperature program started at 90 °C, held for 2 min, then it increased to 130 °C at 15 °C/min and to 290 °C at 4 °C/min with a final holding time of 15 min. Ultrapure helium was used as carrier gas and nitrogen was the make-up gas. Calibration straight lines used for the quantification can be found in the supplemental information (Figs. 3–4). Limits of detection and quantification were 0.0019 and 0.0044 μM for CPF, 0.0045 and 0.0066 μM for CFT and 0.0034 and 0.0047 μM for PMT. Coefficients of variance (CV) calculated to test reproducibility ranged between 11 % and 16 % (CPF and PMT 11 %; CFT 16 %).

2.6. Transwell data analysis

From apical to basolateral transport (A-B transport), initially cumulative amount permeated was calculated followed by flux which is nanomolar passed per cm^2 surface area for all three chemicals to observe the increase in permeation with time. Further, the apparent permeability coefficient of endothelial monolayer was calculated ($P_{app\ A\text{-}B}$) in centimetres/sec (cm/s) that is (Eq. 4),

$$P_{app \quad A-B} = \frac{V_b}{AC_{a0}} * \frac{\Delta C_b}{\Delta t} \tag{4}$$

where V_b is the volume in basolateral compartment, A is the surface area of filter membrane, C_{a0} is the initial concentration in apical compartment, $\Delta C_b/\Delta t$ concentration change over time in basolateral compartment.

The formula used for calculating permeability for basolateral to apical compartment ($P_{app\ B\text{-}A}$) was (Eq. 5),

$$P_{app \quad B-A} = \frac{V_a}{AC_{b0}} * \frac{\Delta C_a}{\Delta t} \tag{5}$$

where V_a is the volume in apical compartment, C_{b0} is the initial concentration in basolateral compartment, $\Delta C_a/\Delta t$ concentration change over time in apical compartment. Efflux ratio is the inverse of

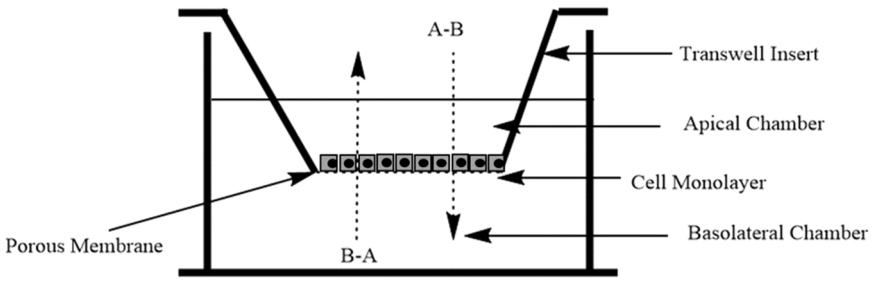

Fig. 1. Setup for bidirectional permeability study using transwell inserts.

uptake that is (Eq. 6),

$$Efflux \quad Ratio = \frac{P_{app \quad BA}}{P_{app, \quad AB}} \tag{6}$$

The efflux ratio was set to 2, all chemicals with a ratio above 2 were considered as the substrate of active transporters while in those below 2, passive diffusion was considered as the primary transport route (Shirasaka et al., 2006; Crowe and Wright, 2012).

2.7. In-vitro in-vivo correlation (IVIVC)

The chemicals' BBB kinetics correlation between the in vitro and in-vivo was established using the IVIVC approach (Abdel-Rahman et al., 2004; Brian Houston and Carlile, 1997; Wilhelm and Krizbai, 2014). The in-vivo data used for establishing correlation was extracted from literature using a webplot (Abdel-Rahman et al., 2004; Brian Houston and Carlile, 1997; Wilhelm and Krizbai, 2014). First, log BB (blood-brain) was calculated using Eq. 7 which represents the ratio of chemical concentration between the brain and plasma. Second, we estimate the log of apparent permeability coefficient from our in-vitro data (Papp $_{A\text{-}B}$) that represent the ratio of intracellular chemical concentrations to media concentration. Then, the log Papp $_{A\text{-}B}$ data against the log BB was fitted using linear regression to calculate the coefficient of determination (r^2).

$$log \quad BB \quad = \quad log(\frac{C_{brain}}{C_{blood/plasma}}) \tag{7}$$

Here C_{brain} refers to the concentration in the brain and $C_{blood/plasma}$ refers to the concentration quantified in blood or plasma.

Velez et al. calculated the AUC (area under curve) in brain and blood upon the oral administration of PMT in rats (Tornero-Velez et al., 2012). For calculating log BB, trans isomer was used by the author but in our in-vitro study, the PMT used was the mixture of cis+trans with more contribution from trans isomer (55–75 % Trans-Isomer). For the CFT, data from rats based on oral administration of 20 mg/Kg BW was used. AUC reported by the author for 0–24 h was taken for plasma and brain. Since the published article contained AUC in several parts of the brain (hypothalamus, striatum, frontal cortex and hippocampus), cumulative AUC was taken for calculating log BB (Rodríguez et al., 2018). A study by Khokhar et al. at the dose of 0.6 μg calculated the brain and plasma concentration in the rat at 4 h. BB (cbrain/cplasma) for CPF was directly extracted from the article published by Poet et al. on the PBPK/PD model. The author has mentioned that this BB was used to validate multiple studies for rat. This value was taken since it has been used by multiple authors irrespective of the dose used in animal (Timchalk et al., 2002; Lowe et al., 2009; Poet et al., 2014) and further it was converted to logarithmic for equivalency to log BB (Poet et al., 2014).

2.8. RNA isolation and cDNA synthesis

The RNA was extracted from cells cultured on the transwell inserts after treatment with the chemicals for 5 h. The experiment was done in triplicate. Total RNA was extracted and isolated from cells using a speedtools Total RNA Extraction Kit (Biotools, Madrid, Spain) as per the manufacture's protocol. RNA was quantified and measured to check purity using a spectrophotometer at the UV absorbance of 260–280 nm (Nanodrop UV-Vis Spectrometer, Thermo Scientific, USA). RNA quality was evaluated by electrophoresis on a 1 % denaturing agarose gel. Using 1 μg of total RNA from each sample, RNA was reverse transcribed by using the GeneAmp PCR System 2700 Thermal Cycler (Applied Biosystems™) for 60 min at 42 °C for reversing transcript, 5 min at 95 °C to inactivate the Reverse Transcriptase and an ultimate 4 °C maintenance.

2.9. Real time PCR (RT-PCR)

The expression of genes (primer shown in Table 1) involved in maintaining tight and adherens junction was evaluated (occludin: OCLN, zona occludens: ZO1, claudin 1: CLDN1, claudin 5: CLDN5, and vascular endothelial cadherins: CDH5) by quantitative RT-PCR in accordance with the manufacturer protocol using a Maxima SYBR Green/ROX qPCR Master Mix (2X) kit (ThermoFisher Scientifics, Waltham, USA). For normalized expression, housekeeping genes (GAPDH) was used. qPCR was performed using Rotor-gene Q Real-Time PCR cycler (Qiagen Inc, U.S.). Samples were tested per triplicate and negative controls (0.1 % DMSO) were also run for each assay. At the end of PCR cycle, heat dissociation protocol was used to analyse the PCR product to confirm that SYBR green dye detects only a single PCR product. The threshold cycle (Ct) was calculated using Rotor-Gene Q 2.0 software for identifying fluorescent signals above noise during the early amplification cycle. The relative expression of target genes was calculated with respect to GAPDH following the $2^{-\Delta\Delta Ct}$ method and it was compared with the control (GAPDH).

2.10. Statistical analysis

All the experiments were performed in triplicate using cells from at least three independent batches. Data was presented as mean ± SD. Significant differences between groups were analysed using one-way analysis of variance (ANOVA) followed by the Dunette test. Homogeneity of variance was analysed using Levene's test. Kruskal-Walis test was conducted when variance was not homogenous. A p value of less than 0.05 was considered significant. The analysis was done with Graphpad Prism 9.3.1 software (Graphpad software, San Diego, CA, USA) and R studio version 2022.02.2 + 461 (Boston, U.S.).

3. Results

3.1. PMT, CFT and CPF significantly altered cell growth and survival

HCMEC/D3 cells were treated with different concentrations of CPF (0, 1, 5, 10, 15, 30 and 60 μM), PMT (0, 1, 50, 100, 200, 600, and 800 μM), and CFT (0, 50, 100, 200, 600, and 800 μM) for 24 h. Cells were cultured for 2–3 days on 48 well plate before exposure. Low to high concentrations were selected for PMT and CFT to understand the BBB toxicity and then selected from multiple doses for further experimentation. For CPF, there were few in-vitro studies available, so the concentration close to the published studies were taken (Yang et al., 2001a, 2001b). Results were expressed as mean ± SD in triplicate (Fig. 2). In PMT, the cell viability decreased from 1 μM to 200 μM significantly up to 78 % and then at higher concentrations (600 and 800 μM), a slight increase was seen but it was not significant. In the case of CFT, viability

Table 1
Primer sequence of tight junction genes used in the RT-PCR experiment.

Primer Name	Oligo Sequence Forward	Oligo Sequence Reverse
Occludin (OCLN)	CAGGAACCGAGAGCCAGGT	ATAAACCAATCTGCTGCGTCCTA
Zona Occludens (ZO1)	CAGCCGGTCACGATCTCCT	TCCGGAGACTGCCATTGC
Claudin 1 (CLDN1)	GTTGGGCTTCATTCTCGC	CTGCACCTCATCGTCTTCC
Claudin 5 (CLDN5)	CTGCTGGTTCGCCAACATT	TGCGACACGGGCACAG
VE-Cadherin (CDH5)	ACCAGGACGCTTTCACCAT	AAAGGCTGCTGGAAAATGGG
Glyceraldehyde-3-phosphate dehydrogenase (GAPDH)	GAAGGTGAAGGTCGGAGTCAAC	CAGAGTTAAAAGCAGCCCTGGT

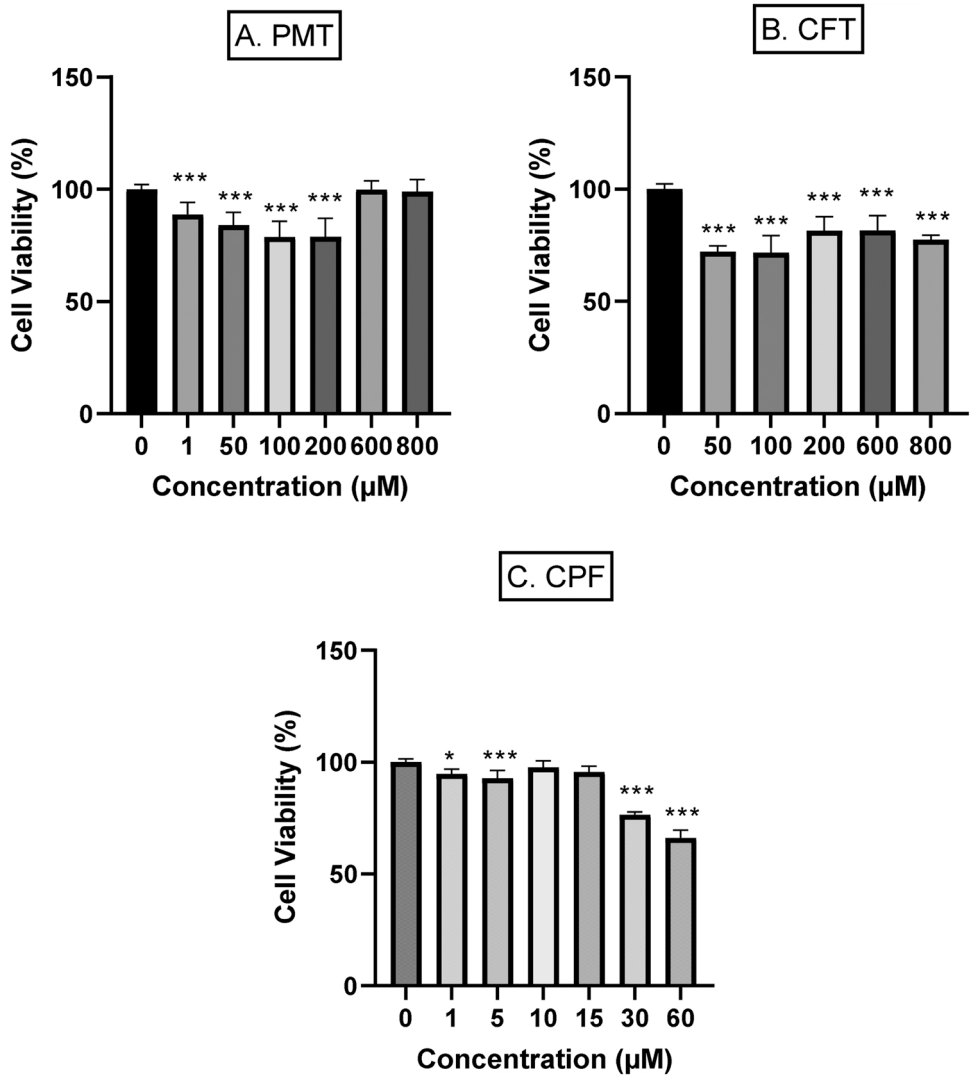

Fig. 2. Cell Viability of three chemicals. A represents PMT, B represents CFT and C represents CPF. X axis represents concentration in μM and y axis represents cell viability. Data is represented as mean ± SD of at least three independent experiment. Differences relative to the control were analysed by one-way ANOVA followed by Dunnett test with p value < 0.05 as significant.

decreased to 78 % at 100 and at 200 uM, it increased slightly compared to control. At 800 uM, cell viability was lower than the control. CPF showed a statistically significant decrease in viability at 1 and 5 μM up to 92 %. At 30 and 60 μM, viability decreased further below 70 %.

3.2. Integrity of BBB monolayer with time through TEER

The chemical transport through intercellular spaces depends on the integrity of BBB. The TEER assay was conducted to check the integrity of monolayer for simulating the same condition as human BBB. An increase in TEER was seen from day 1 to day 5 and then leveled off until day 7 (Fig. 3). A decrease in electrical resistance was observed after exposure to the chemicals especially CPF. The decrease was insignificant for PMT and CFT (Fig. 1 in supplementary file).

3.3. Permeability across BBB and the role of active transport

Based on cell viability results, dosing was chosen for all three compounds with one dose for the viability of more than 70 % and other above 80 % viability, (PMT: 50 and 200 μM, CFT: 100 and 600 μM, CPF: 10 and 30 μM). This was done to check if concentration has some effect on permeation property, especially due to cell death. Dosing was given

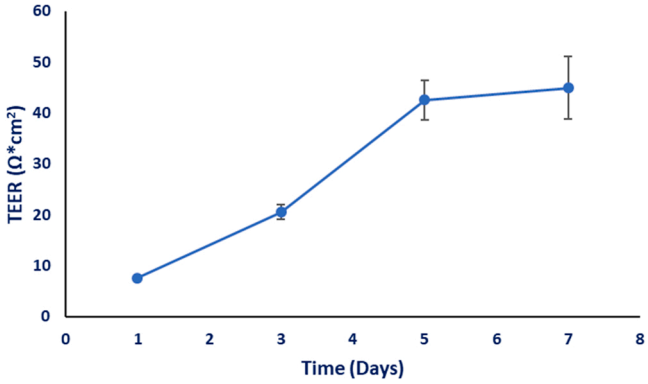

Fig. 3. TEER for Transwell plate after growing the cells for 7–8 days. X axis represent time in days and y axis represent TEER. Data is represented as mean ± SD of at least three independent experiment.

after culturing the cells for 7 days on transwell inserts. The cumulative amount permeated per cm^2 remained almost similar for PMT and CFT whereas for CPF, the increase was minimal (Fig. 2 in supplementary

file). At 30 μM for CPF, the amount permeated was slightly more than 10 μM, but the increase was not significant (less than 1.5-fold). It was seen that cumulative amount and hence the permeability was independent of the concentration. The flux was in-line with the cumulative amount with almost no change based on concentration for PMT and CFT and a slight variation in the case of CPF. Papp $_{A-B}$ and Papp $_{B-A}$ were calculated for all three compounds. Since the $Papp_{A-B}$ was independent of the concentration, the mean $Papp_{A-B}$ was calculated for all three chemicals. P_{app} more than 10^{-5} is considered to be highly permeable which is the case of CPF among all three chemicals. Both PMT and CFT are low permeable compounds (CPF>CFT>PMT; Fig. 4). The efflux ratio was less than 2 for CPF (10 and 30 μM) and PMT (50 and 200 μM) but for CFT only at higher concentration (600 μM), the efflux ratio was more than 2 (Fig. 5).

3.4. Physicochemical properties and IVIVC evaluation

The performance of the in-vitro BBB model was compared with the in-vivo values to discriminate the ability to predict chemical permeation. The log BB was in good correlation with the log Papp value with a correlation coefficient of 0.82 calculated using the Pearson method (Fig. 6). The permeability values were then classified to determine the chemical ranking from best to the worst ability for crossing the BBB. This was in the opposite trend with the lipophilicity of the compound. CPF has the lowest lipophilicity, log P = 4.96, but the highest ability to cross both in-vitro and in-vivo, followed by CFT (log P = 5.95) and PMT (log P = 6.5). Thus, chemicals with log P value of less than 5 could permeate better than chemicals having log P above 5. Fig. 6

3.5. Endothelial gene expression of tight junction present in BBB

The gene expression profiles were assessed using HCMEC/D3 cell lines after treatment for 5 h with each chemical. Cells were grown on a transwell insert for 7 days before starting the experiment. Several genes associated with the expression of tight junction and adherens protein are responsible for limiting the permeation of xenobiotics and contribute to high TEER value (Lopez-Ramirez et al., 2013; Lochhead et al., 2020). In the case of PMT, a significant decrease in CDH5 gene expression was observed after treatment at 50 and 200 μM (Fig. 7). Downregulation was observed for other genes but was not statistically significant. CFT showed significant downregulation of ZO1 gene expression at 100 and 600 μM (Fig. 8). At 100 μM, downregulation of the CLDN5 gene was observed but not at 600 μM. The OCLN gene was down regulated in CPF-treated cells at both 10 and 30 μM (Fig. 9). The other genes did not show any significant change in their expression.

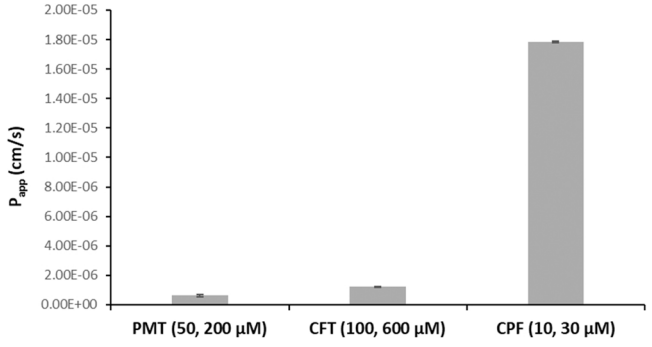

Fig. 4. P_{app} for all three compounds for apical to basolateral transport. Data is represented as mean ± SD of at least three independent experiment. SD here represents the average P_{app} at two concentration for each compound: PMT: 50 and 200 μM, CFT: 100 and 600 μM, CPF: 10 and 30 μM).

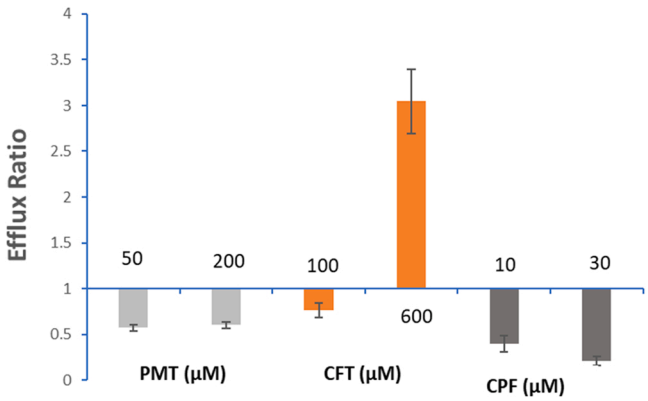

Fig. 5. Efflux Ratio for several chemicals, PMT represents permethrin, CFT: Cyfluthrin and CPF: Chlorpyrifos. Bi-Permeability assay was done to identify and quantify the level of active efflux (B-A/A-B). The CFT at higher concentration with efflux ratio of more than 2 indicates that compound may be subject to active efflux. Data is represented as mean ± SD of at least three independent experiment.

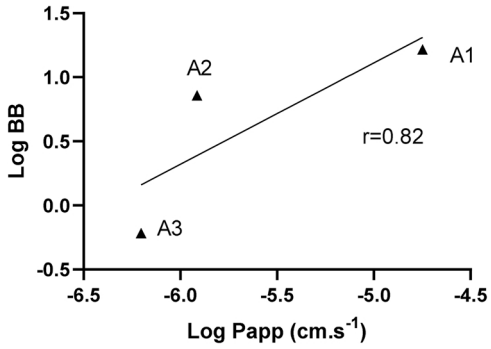

Fig. 6. Linear regression plot for in-vitro Papp value with in-vivo log BB correlation (IVIVC) for 3 chemicals. Pearson correlation was used for calculating the correlation coefficient (r). A1, A2 and A3 represent the three chemicals, PMT, CFT and CPF.

4. Discussion

The present study utilizes an in-vitro model of the human BBB to examine the permeation of three insecticides (CPF, PMT and CFT). Three immortalized human BBB cell lines are BB19, NKIM-6, and HCMEC/D3. BB19 use is limited due to high sucrose permeability and with NKIM-6, limited bidirectional study has been conducted (Poller et al., 2008). HCMEC/D3 cell lines were selected for the study due to their easy growth and widespread use by scientists to study transport mechanisms (Weksler et al., 2013b; Poller et al., 2008). CPF exposure at 10 and 30 μM had the highest potential to compromise the BBB integrity (Fig. 9). This result was in concordance with the literature finding where CPF was found to have a high Papp value of $2.3 \pm 0.22 * 10^{-4}$-6.0 $\pm 0.49 * 10^{-5}$ m/min with control media and astrocyte conditioned media (Yang et al., 2001a). Moreover CPF had a much higher Papp value than the other chemicals (Fig. 4). The reason behind the high permeation of the CPF can be its inherent physicochemical properties. CPF has a log P value less than 4.96 and lower molecular weight of 350.6, hydrogen bond donor count 0 and hydrogen bond acceptor count of 5 (National Center for Biotechnology Information, 2022a). CPF follows all parameters for Lipinskiś rule making it a good candidate for higher permeation. Additionally, our genetic expression result suggests that CPF interaction with tight junction proteins may play a pivotal role in BBB disruption. OCLN gene was down expressed significantly at 10 and 30 μM compared to control (0.1 % DMSO). OCLN is a tight junction

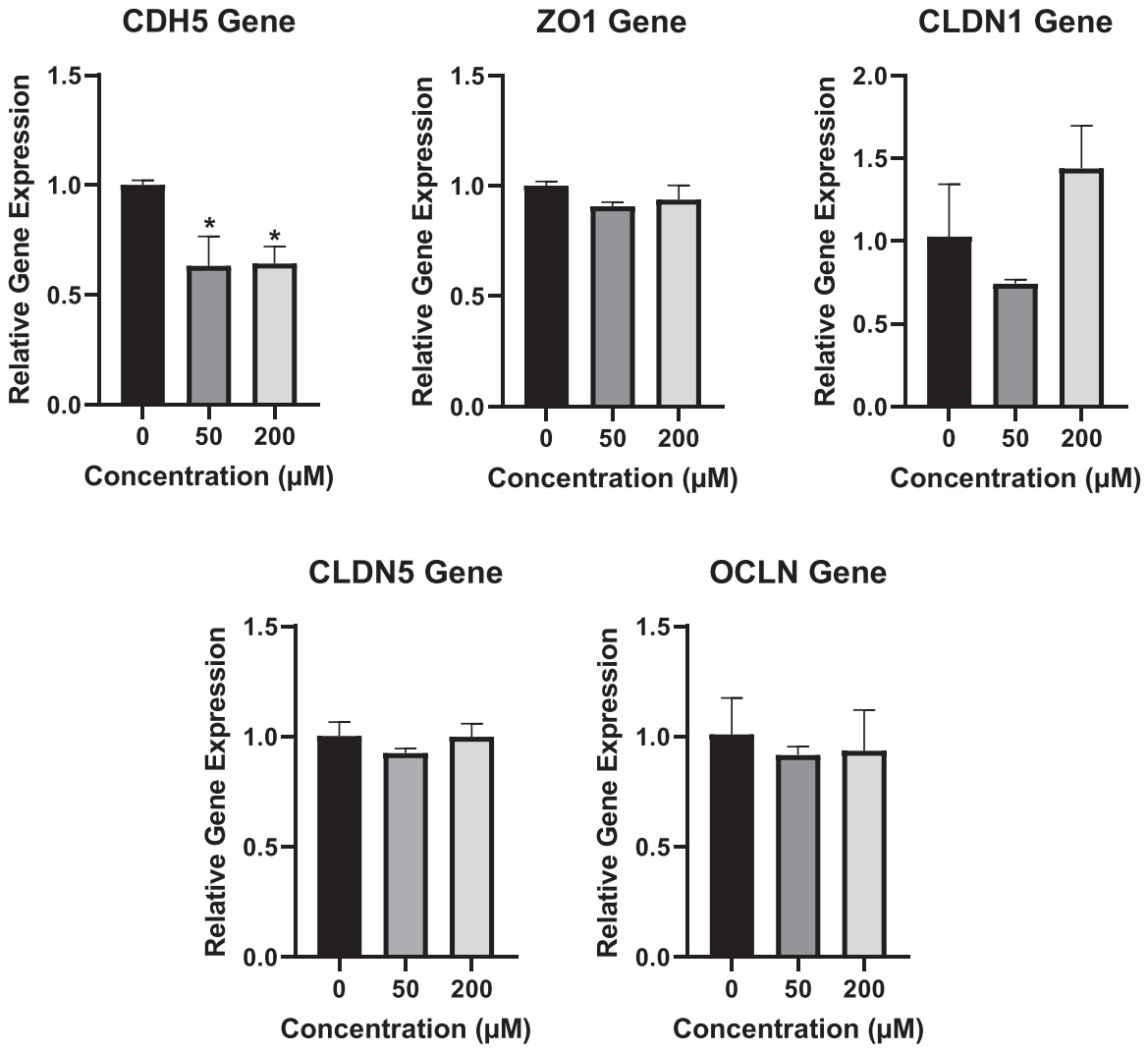

Fig. 7. BBB genetic expression after exposure to PMT. The genes represented in the figure are OCLN (occludin gene), CLDN1 (claudin 1), CDH5 (vascular endothelial cadherin), ZO1 (zona occludens), and CLDN5 (claudin-5). Data is represented as mean ± SD of three independent experiment. Differences relative to the control was analysed by one-way ANOVA followed by Dunnett test with p value < 0.05 as significant.

transmembrane protein and a key structural component of BBB (Yuan et al., 2020). Many studies have indicated that disruption in OCLN gene can serve as an important biomarker for BBB permeability and integrity (Yuan et al., 2020). The OCLN gene is being regulated by several signalling pathways like nuclear factor-kappa B, mitogen-activated protein kinase (MAPK), protein kinase C, RhoK, and ERK1/2 (Yuan et al., 2020). So, it might be possible that CPF might downregulate OCLN via these pathways. This study demonstrated that OCLN down-regulation was in line with the significant reduction seen in TEER after CPF exposure (Fig. 1 in supp file) and also decreased cell viability (Fig. 2).

PMT was found to be a low permeable compound at the tested concentrations in our experiment. PMT has a log P value of 6.5 and a molecular weight of 391.3 violating one criterion for the Lipinski rule (National Center for Biotechnology Information, 2022b). The efflux ratio of PMT was found to be less than 2, suggesting that PMT was not a substrate for active transport. This observation suggests PMT has only passive permeation. The point worth mentioning is that literature suggests BBB penetration increase with lipophilicity upto a certain point, but very high log P might lead to a decrease in permeation. The PMT might be trapped in the membrane due to reduced flux, poor partitioning and hydrophobic bonding (Mortuza et al., 2019). The genetic expression result showed significant downregulation of CDH5 gene (Fig. 7). CDH5 is an important component in the vascular system and is responsible for assembly of BBB architecture and adherens Junction. CDH5 is exclusive to endothelial cells and aids in communicating with the cells of similar type. One study established that CDH5, along with other TJs proteins affect the integrity of BBB (Weber, 2012). It may be possible that single downregulation of CDH5 cannot completely disrupt BBB integrity, that's why also no significant change in TEER was observed at the tested concentrations of PMT. To further understand this, neuroinflammatory cytokines and other potential biomarkers like TNFα (Tumor necrosis factor) and IFNγ (Interferon gamma) should be measured to clarify this aspect, which indirectly concerns the maintenance of barrier integrity (Lopez-Ramirez et al., 2013). It may be possible that PMT being a low permeable molecule for human at the selected doses, still it can affect the brain indirectly. Some environmental chemicals cause neurotoxicity by altering the gut microbiota composition which in turn produces neuro-reactive microbial metabolites (short chain fatty acids) and neurotransmitters (GABA, serotonin etc.) (Dempsey et al., 2019). A similar phenomenon may be happening with PMT, but detailed understanding requires further experiments.

CFT was also low permeable, but the permeability coefficient was more than PMT. CFT has log P value of 6.2 and molecular weight of 434.3 violating one criterion for Lipinski rule similar to PMT. In our study, CFT was found to be low-medium permeable with a Papp value of $1.22 * 10^{-6}$ ($cm.s^{-1}$) and was found to be a concentration-dependent

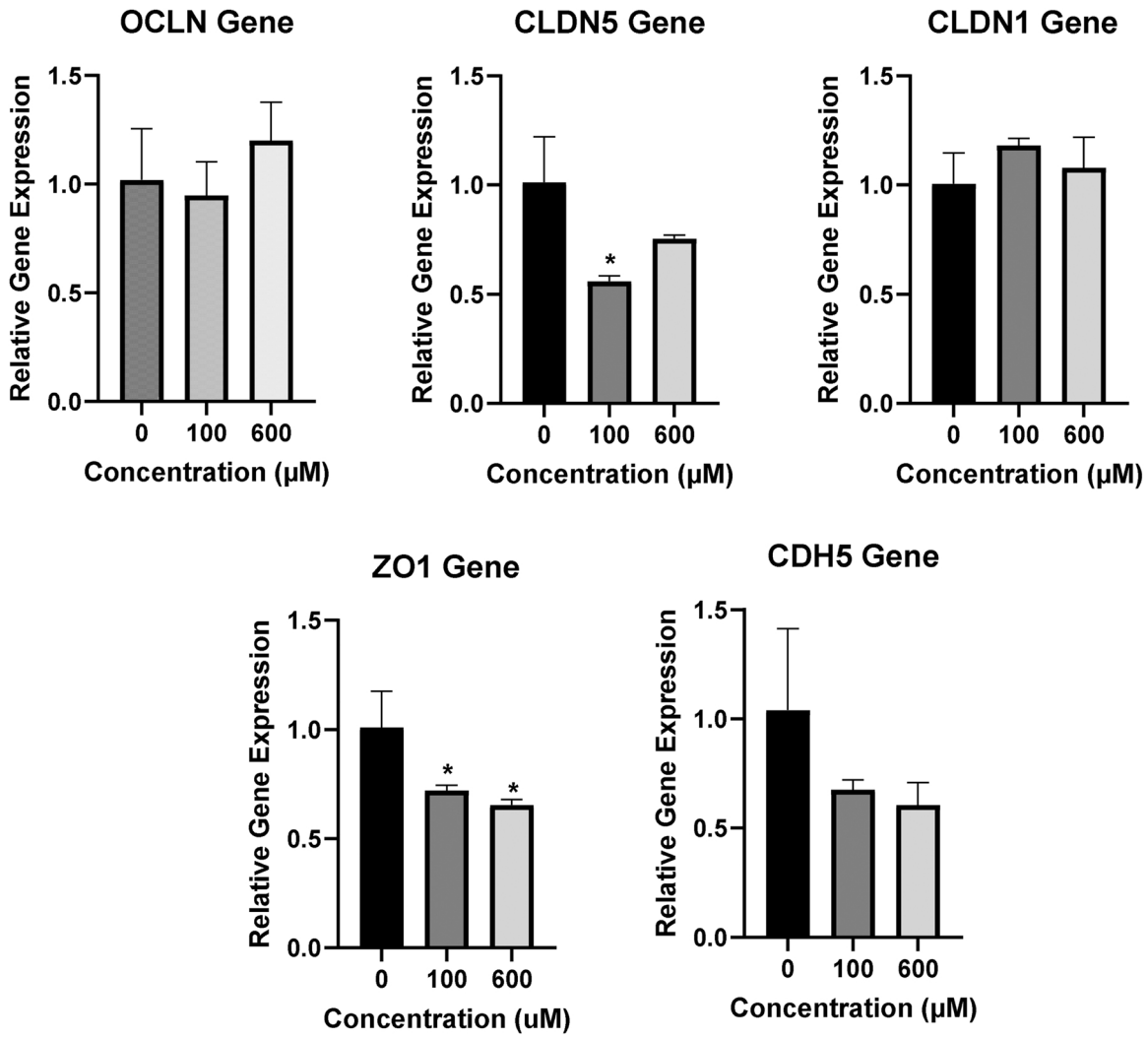

Fig. 8. Genetic expression of CFT. The genes represented in the figure are OCLN (occludin gene), CLDN1 (claudin 1), CDH5 (vascular endothelial cadherin), ZO1 (zona occludens), and CLDN5 (claudin-5). Data is represented as mean ± SD of three independent experiment. Differences relative to the control was analysed by one-way ANOVA followed by Dunnett test with p value < 0.05 as significant.

substrate for active transport (discussed below). At the tested concentration, CFT did not show any alteration in the integrity (shown by no significant change in resistance). However, CFT exposure to the cells resulted in the significant downregulation of the ZO1 gene at both concentrations whereas CLDN5 was downregulated only at lower concentration (100 μM). Downregulation of CLDN5 at 100 μM did not impact the permeability as the cumulative amount permeated was found to be similar at both the concentrations (Fig. 2 in supp file). ZO1 is considered the support for signal transduction protein and recognition protein for tight junction placement. A study demonstrated that alteration in ZO1 could result in tight junction disorganization (Jiao et al., 2011). So, It may be possible that downregulation of ZO1 impacted BBB tight junction and consequently increased permeation (Jiao et al., 2011). However, the major tight junction proteins directly involved in the BBB are CLDN5, CLDN3 and OCLN (Luissint et al., 2012). Further studies need to be conducted to understand the activation of pathways associated with ZO1 at the BBB. For instance, in a rat study, a seizure was associated with downregulation of ZO-1, claudins and occludin at the BBB, resulting in glutamate production (Lochhead et al., 2020; Rempe et al., 2018). This increased glutamate activated the cytosolic phospholipase A2, by activation of enzyme matrix metalloproteinase (MMP)− 2 and MMP9, leading to further aggravation of BBB leakage (Lochhead et al., 2020; Rempe et al., 2018). Such aggravation of BBB leakage could play a role in altering Papp value.

Apart from passive diffusion, active transport also plays a vital role in the permeation of xenobiotics. Transporters like P-GP and Breast Cancer Resistant Protein (BCRP) play a significant role in active transport at BBB. We calculated the efflux ratio to understand the active transport. The efflux ratio for CPF was found to be lower than 2, suggesting that CPF may not be the substrate for active transport in our in-vitro model. This result was not in agreement with the rat study by Lanning et al (Lanning, 1996). where author demonstrated CPF has the ability to interact and increase the expression of P-GP in several organs (Lanning, 1996). The study also suggested that CPF can be pumped outside the BBB, in another sense, the efflux ratio (P_{app} B-A/ P_{app} A-B) should be high. However, the differences in both results could be explained by the fact that CPF can be metabolized to CPF-oxon by CYP enzymes which could act as a substrate for P-GP (Yang et al., 2001b). Moreover the incubation time with the chemical was 5 h in our study which may be shorter than the time required for energy-mediated transport as a time-dependent xenobiotic transport may happen which has also been observed with other chemicals (Di Leo et al., 2021). Moreover, it has been shown that the efflux ratio can vary based on the concentration used for flux (Poller et al., 2008). For instance, a candidate drug for treating Parkinson's disease showed a varied efflux ratio with several concentration ranging from 1 to 10 μM (Liu et al., 2014). A similar kind

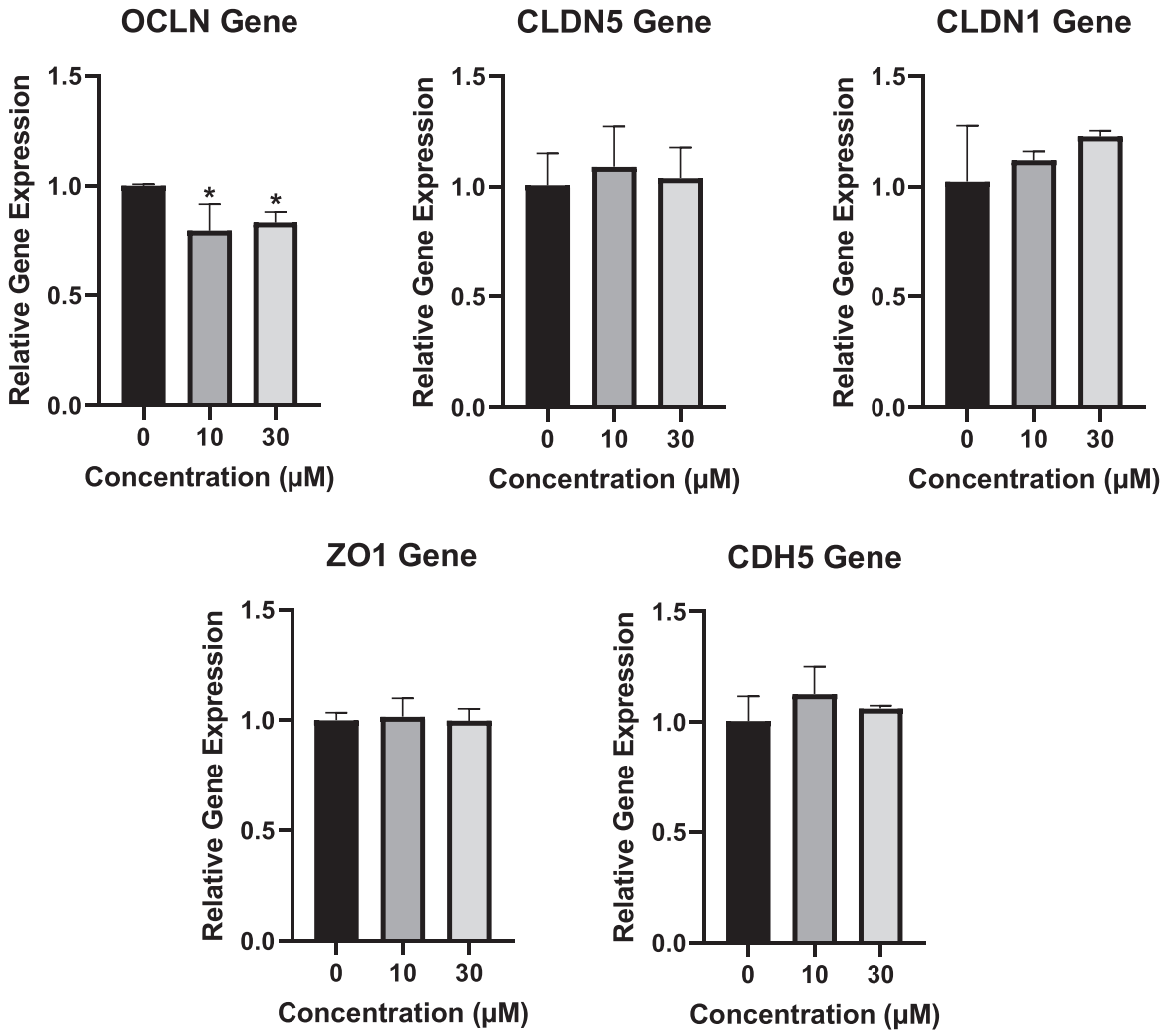

Fig. 9. Genetic expression of CPF. The genes represented in the figure are OCLN (occludin gene), CLDN1 (claudin 1), CDH5 (vascular endothelial cadherin), ZO1 (zona occludens), and CLDN5 (claudin-5). Data is represented as mean ± SD of three independent experiment. Differences relative to the control was analysed by one-way ANOVA followed by Dunnett test with p value < 0.05 as significant.

of phenomenon was seen in the case of CFT, where at a particular concentration (600 μM), the efflux ratio was found to be more than 2 making it a substrate for active transport (Saaby and Brodin, 2017). Overall study suggests that the efflux ratio could be dose and time-dependent, and formation of its active metabolites. An in-vitro study using immortalized rat brain endothelium 4 (RBE4) cell line showed that CPF concentration did not change after blocking the P-GP using VPM (Verapamil), indicating CPF is not a substrate for P-GP (Yang et al., 2001b). Further study needs to be done to understand the active transport role for CPF and its metabolite. The Papp value does not take into account the saturable nature of the transporter, so the efflux ratio can vary based on the concentration used for flux (Liu et al., 2014). In our study, PMT was not found to be the substrate for active transport. We have not found any study in the literature regarding BBB permeation where it was shown that whether or not PMT is a substrate for the active transport. This is the first study to report about active transport of PMT and this data can be valuable for understanding the toxicokinetic of this chemical.

In-vitro models are valuable tools for screening chemicals and drug compounds allowing fast screening and helping in reducing animal usage (Curzer et al., 2016). The ultimate step of our study was to correlate the in-vitro results with the published in-vivo data from rats or mice. The conventional IVIVC approach was used based on a linear regression between log BB and log Papp. The good correlation was observed with r value of 0.812 (Fig. 6). Thus, the in-vitro model seemed to display a good prediction three chemicals. The reason for conducting IVIVC is to establish confidence that in-vitro study can provide quantitative BBB permeation value and act as alternative for the in-vivo. However, this was a limited case study and to conclude in general, we need data for multiple short-acting and long-acting chemicals. In future, the Papp data calculated in our in-vitro study could be used for building permeability limited physiologically based pharmacokinetic models (PBPK) for human considering both the A-B and B-A transport. Such kind of in-silico models utilizing the in-vitro data from human cell lines are promising to reduce animal exploitation in research. For instance, permeability limited human brain and CSF PBPK model was developed utilizing the in-vitro data for paracetamol and phenytoin (Gaohua et al., 2016).

However, our study has a few limitations like plasma protein binding was not considered. It may be possible that the binding of these chemicals with the albumin and plasma proteins can impact their permeation potential (Amaraneni et al., 2016). Chemicals like PMT, CFT and CPF are extensively oxidized and hydrolysed by the rat and human hepatic microsomal enzymes (Lanning, 1996; Scollon et al., 2009). It may be possible that PMT, CFT, and CPF catabolism by microsomal enzymes could produce metabolites affecting the BBB. Subsequent in-vitro models can be improved by including the albumin in the permeation study and checking the permeation for both chemical and metabolite.

5. Conclusion

In the present study, we calculated the Papp value, both influx (A-B) and efflux (B-A) for CPF, PMT and CFT using HCMEC/D3 cell lines. The results of the present study showed that CPF has the highest potential to permeate the BBB of the three chemicals examined. This compound disrupts the tight junction independently of the concentration, but we have checked for only two concentrations. The high permeation can be due to disturbances in the BBB tight junction as evidenced by the genetic expression and change in resistance. Further studies like western blot or immunocytochemical staining for CPF can provide additional evidence regarding BBB disruption. The efflux ratio of CFT was found to increase at higher concentration pointing towards concentration-dependent active transport. In the case of PMT, no active transport was observed, and this is the first study to report this data using human cell lines. Further, IVIVC pointed towards the validity of the in-vitro results. Such kind of rich in-vitro data can be used in future to build a brain-specific PBPK model to understand the risk.

CRediT authorship contribution statement

Deepika Deepika: Conceptualization, Methodology, Data Analysis, and writing; **Natalia Bravo:** Analysis by GC-ECD, writing about GC-ECD, and review; **Roser Esplugas:** Supervision, and Review; **Marco Capodiferro:** Writing about GC-ECD and review; **Raju Prasad Sharma:** Supervision and Review, **Marta Schuhmacher:** Supervision and Review; **Joan O. Grimalt:** Supervision, Analysis by GC-ECD, writing, and Review; **Jordi Blanco:** Supervision, Conceptualization, Data Analysis, Review and Revision, **Vikas Kumar:** Supervision, Conceptualization, Methodology, Data Analysis, writing, review and revision.

Declaration of Competing Interest

The authors declare the following financial interests/personal relationships which may be considered as potential competing interests: Marta Schuhmacher reports financial support was provided by European Union.

Data availability

The raw dataset produced or analysed during current study can be available from the corresponding author by a reasonable request.

Acknowledgement

This study was financially supported by Marie Skłodowska-Curie “Neurosome Project” under the grant agreement No. 766251. This publication reflects only the authors’ views. The Community and other funding organizations are not liable for any use made of the information contained therein.

Appendix A. Supporting information

Supplementary data associated with this article can be found in the online version at doi:10.1016/j.neuro.2022.09.010.

References

Abbott, N.J., 2013. Blood–brain barrier structure and function and the challenges for CNS drug delivery. J. Inherit. Metab. Dis. 36, 437–449. https://doi.org/10.1007/s10545-013-9608-0.

Abdel-Rahman, A., Abou-Donia, S.M., El-Masry, E.M., Shetty, A.K., Abou-Donia, M.B., 2004. Stress and combined exposure to low doses of pyridostigmine bromide, DEET, and permethrin produce neurochemical and neuropathological alterations in cerebral cortex, hippocampus, and cerebellum. J. Toxicol. Environ. Heal. Part A 67, 163–192. https://doi.org/10.1080/15287390490264802.

Abu-Qare, A.W., Abou-Donia, M.B., 2003. Combined exposure to deet (n, n-Diethyl-m-Toluamide) and permethrin: pharmacokinetics and toxicological effects. J. Toxicol. Environ. Health Part B Crit. Rev. 6, 41–53. https://doi.org/10.1080/10937400390155481.

Akamine, Y., Yasui-Furukori, N., Uno, T., 2019. Drug-drug interactions of P-Gp substrates unrelated to CYP metabolism. Curr. Drug Metab. 20, 124–129. https://doi.org/10.2174/1389200219666181003142036.

Amaraneni, M., Sharma, A., Pang, J., Muralidhara, S., Cummings, B.S., White, C.A., Bruckner, J.V., Zastre, J., 2016. Plasma protein binding limits the blood brain barrier permeation of the pyrethroid insecticide, deltamethrin. Toxicol. Lett. 250–251, 21–28. https://doi.org/10.1016/j.toxlet.2016.03.006.

Breckenridge, C.B., Holden, L., Sturgess, N., Weiner, M., Sheets, L., Sargent, D., Soderlund, D.M., Choi, J.-S., Symington, S., Clark, J.M., et al., 2009. Evidence for a separate mechanism of toxicity for the type I and the type II pyrethroid insecticides. Neurotoxicology 30, S17–S31. https://doi.org/10.1016/j.neuro.2009.09.002.

Brian Houston, J., Carlile, D.J., 1997. Prediction of hepatic clearance from microsomes, hepatocytes, and liver slices. Drug Metab. Rev. 29, 891–922. https://doi.org/10.3109/03602539709002237.

Burke, R.D., Todd, S.W., Lumsden, E., Mullins, R.J., Mamczarz, J., Fawcett, W.P., Gullapalli, R.P., Randall, W.R., Pereira, E.F.R., Albuquerque, E.X., 2017. Developmental neurotoxicity of the organophosphorus insecticide chlorpyrifos: from clinical findings to preclinical models and potential mechanisms. J. Neurochem. 142, 162–177. https://doi.org/10.1111/jnc.14077.

Crowe, A., Wright, C., 2012. The impact of P-glycoprotein mediated efflux on absorption of 11 sedating and less-sedating antihistamines using Caco-2 monolayers. Xenobiotica 42, 538–549. https://doi.org/10.3109/00498254.2011.643256.

Curzer, H.J., Perry, G., Wallace, M.C., Perry, D., 2016. The three Rs of animal research: what they mean for the Institutional Animal Care and Use Committee and why. Sci. Eng. Ethics 22, 549–565. https://doi.org/10.1007/s11948-015-9659-8.

Dempsey, J.L., Little, M., Cui, J.Y., 2019. Gut microbiome: an intermediary to neurotoxicity. Neurotoxicology 75, 41–69. https://doi.org/10.1016/j.neuro.2019.08.005.

Di Leo, N., Moscato, S., Borso’, M., Sestito, S., Polini, B., Bandini, L., Grillone, A., Battaglini, M., Saba, A., Mattii, L., et al., 2021. Delivery of thyronamines (Tams) to the brain: a preliminary study. Molecules 26, 1616. https://doi.org/10.3390/molecules26061616.

Eaton, D.L., Daroff, R.B., Autrup, H., Bridges, J., Buffler, P., Costa, L.G., Coyle, J., McKhann, G., Mobley, W.C., Nadel, L., et al., 2008. Review of the toxicology of chlorpyrifos with an emphasis on human exposure and neurodevelopment. Crit. Rev. Toxicol. 38, 1–125. https://doi.org/10.1080/10408440802272158.

EU-Wide, n.d., Ban of Chlorpyrifos and Chlorpyrifos-Methyl - Eurofins Scientific. ⟨https://www.eurofins.de/food-analysis/food-news/food-testing-news/eu-wide-ban-of-chlorpyrifos-and-chlorpyrifos-methyl/⟩.

Fluegge, K.R., Nishioka, M., Wilkins, J.R., 2016. Effects of simultaneous prenatal exposures to organophosphate and synthetic pyrethroid insecticides on infant neurodevelopment at three months of age. J. Environ. Toxicol. Public Health 1, 60–73. https://doi.org/10.5281/zenodo.218417.

Gaohua, L., Neuhoff, S., Johnson, T.N., Rostami-Hodjegan, A., Jamei, M., 2016. Development of a permeability-limited model of the human brain and cerebrospinal fluid (CSF) to integrate known physiological and biological knowledge: estimating time varying csf drug concentrations and their variability using in vitro data. Drug Metab. Pharmacokinet. 31, 224–233. https://doi.org/10.1016/j.dmpk.2016.03.005.

Gericke, B., Römermann, K., Noack, A., Noack, S., Kronenberg, J., Blasig, I.E., Löscher, W., 2020. A face-to-face comparison of Claudin-5 transduced human brain endothelial (HCMEC/D3) cells with porcine brain endothelial cells as blood-brain barrier models for drug transport studies. Fluids Barriers CNS 17, 53. https://doi.org/10.1186/s12987-020-00212-5.

Goel, A., Dani, V., Dhawan, D.K., 2005. Protective effects of zinc on lipid peroxidation, antioxidant enzymes and hepatic histoarchitecture in chlorpyrifos-induced toxicity. Chem. Biol. Interact. 156, 131–140. https://doi.org/10.1016/j.cbi.2005.08.004.

Guo, J., Zhang, J., Wu, C., Lv, S., Lu, D., Qi, X., Jiang, S., Feng, C., Yu, H., Liang, W., et al., 2019. Associations of prenatal and childhood chlorpyrifos exposure with neurodevelopment of 3-year-old children. Environ. Pollut. 251, 538–546. https://doi.org/10.1016/j.envpol.2019.05.040.

Hoshi, Y., Uchida, Y., Tachikawa, M., Inoue, T., Ohtsuki, S., Terasaki, T., 2013. Quantitative atlas of blood–brain barrier transporters, receptors, and tight junction proteins in rats and common marmoset. J. Pharm. Sci. 102, 3343–3355. https://doi.org/10.1002/jps.23575.

Jiao, H., Wang, Z., Liu, Y., Wang, P., Xue, Y., 2011. Specific role of tight junction proteins Claudin-5, Occludin, and ZO-1 of the blood–brain barrier in a focal cerebral ischemic insult. J. Mol. Neurosci. 44, 130–139. https://doi.org/10.1007/s12031-011-9496-4.

Lanning, C.L., 1996. Chlorpyrifos oxon interacts with the mammalian multidrug resistance protein, P-glycoprotein. J. Toxicol. Environ. Health 47, 395–407. https://doi.org/10.1080/009841096161726.

Li, W., Ehrich, M., 2013. Transient alterations of the blood-brain barrier tight junction and receptor potential channel gene expression by chlorpyrifos. J. Appl. Toxicol. 33, 1187–1191. https://doi.org/10.1002/jat.2762.

Liu, Q., Hou, J., Chen, X., Liu, G., Zhang, D., Sun, H., Zhang, J., 2014. P-glycoprotein mediated efflux limits the transport of the novel anti-Parkinson’s Disease candidate drug FLZ across the physiological and PD pathological in vitro BBB models. PLoS One 9, e102442. https://doi.org/10.1371/journal.pone.0102442.

Lochhead, J.J., Yang, J., Ronaldson, P.T., Davis, T.P., 2020. Structure, function, and regulation of the blood-brain barrier tight junction in central nervous system disorders. Front. Physiol. 11. https://doi.org/10.3389/fphys.2020.00914.

López-Aceves, T.G., Coballase-Urrutia, E., Estrada-Rojo, F., Vanoye-Carlo, A., Carmona-Aparicio, L., Hernández, M.E., Pedraza-Chaverri, J., Navarro, L., Aparicio-Trejo, O. E., Pérez-Torres, A., et al., 2021. Exposure to sub-lethal doses of permethrin is associated with neurotoxicity: changes in bioenergetics, redox markers,

neuroinflammation and morphology. Toxics 9, 337. https://doi.org/10.3390/toxics9120337.

Lopez-Ramirez, M.A., Male, D.K., Wang, C., Sharrack, B., Wu, D., Romero, I.A., 2013. Cytokine-induced changes in the gene expression profile of a human cerebral microvascular endothelial cell-line, HCMEC/D3. Fluids Barriers CNS 10, 27. https://doi.org/10.1186/2045-8118-10-27.

Lowe, E.R., Poet, T.S., Rick, D.L., Marty, M.S., Mattsson, J.L., Timchalk, C., Bartels, M.J., 2009. The effect of plasma lipids on the pharmacokinetics of chlorpyrifos and the impact on interpretation of blood biomonitoring data. Toxicol. Sci. 108, 258–272. https://doi.org/10.1093/toxsci/kfp034.

Luissint, A.-C., Artus, C., Glacial, F., Ganeshamoorthy, K., Couraud, P.-O., 2012. Tight junctions at the blood brain barrier: physiological architecture and disease-associated dysregulation. Fluids Barriers CNS 9, 23. https://doi.org/10.1186/2045-8118-9-23.

Mortuza, T.B., Edwards, G.L., White, C.A., Patel, V., Cummings, B.S., Bruckner, J.V., 2019. Age dependency of blood-brain barrier penetration by Cis- and trans -permethrin in the rat. Drug Metab. Dispos. 47, 234–237. https://doi.org/10.1124/dmd.118.084822.

National Center for Biotechnology Information, 2022a. PubChem compound summary for CID 2730. Chlorpyrifos. ⟨Https://Pubchem.Ncbi.Nlm.Nih.Gov/Compound/Chlorpyrifos⟩.

National Center for Biotechnology Information (2022b). PubChem compound summary for CID 40326, Permethrin. ⟨https://pubchem.ncbi.nlm.nih.gov/compound/Permethrin⟩.

Oliver, G.R., Bolles, H.G., Shurdut, B.A., 2000. Chlorpyrifos: probabilistic assessment of exposure and risk. Neurotoxicology 21, 203–208.

Poet, T.S., Timchalk, C., Hotchkiss, J.A., Bartels, M.J., 2014. Chlorpyrifos PBPK/PD model for multiple routes of exposure. Xenobiotica 44, 868–881. https://doi.org/10.3109/00498254.2014.918295.

Poller, B., Gutmann, H., Krähenbühl, S., Weksler, B., Romero, I., Couraud, P.-O., Tuffin, G., Drewe, J., Huwyler, J., 2008. The human brain endothelial cell line HCMEC/D3 as a human blood-brain barrier model for drug transport studies. J. Neurochem. 107, 1358–1368. https://doi.org/10.1111/j.1471-4159.2008.05730.x.

Rempe, R.G., Hartz, A.M.S., Soldner, E.L.B., Sokola, B.S., Alluri, S.R., Abner, E.L., Kryscio, R.J., Pekcec, A., Schlichtiger, J., Bauer, B., 2018. Matrix metalloproteinase-mediated blood-brain barrier dysfunction in epilepsy. J. Neurosci. 38, 4301–4315. https://doi.org/10.1523/JNEUROSCI.2751-17.2018.

Rodríguez, J.L., Ares, I., Castellano, V., Martínez, M., Martínez-Larrañaga, M.R., Anadón, A., Martínez, M.A., 2016. Effects of exposure to pyrethroid cyfluthrin on serotonin and dopamine levels in brain regions of male rats. Environ. Res. 146, 388–394. https://doi.org/10.1016/j.envres.2016.01.023.

Rodríguez, J.-L., Ares, I., Martínez, M., Martínez-Larrañaga, M.-R., Anadón, A., Martínez, M.-A., 2018. Bioavailability and nervous tissue distribution of pyrethroid insecticide cyfluthrin in rats. Food Chem. Toxicol. 118, 220–226. https://doi.org/10.1016/j.fct.2018.05.012.

Saaby, L., Brodin, B., 2017. A critical view on in vitro analysis of P-glycoprotein (P-Gp) transport kinetics. J. Pharm. Sci. 106, 2257–2264. https://doi.org/10.1016/j.xphs.2017.04.022.

Saunders, M., Magnanti, B.L., Correia Carreira, S., Yang, A., Alamo-Hernández, U., Riojas-Rodriguez, H., Calamandrei, G., Koppe, J.G., Krayer von Krauss, M., Keune, H., et al., 2012. Chlorpyrifos and neurodevelopmental effects: a literature review and expert elicitation on research and policy. Environ. Health 11, S5. https://doi.org/10.1186/1476-069X-11-S1-S5.

Scollon, E.J., Starr, J.M., Godin, S.J., DeVito, M.J., Hughes, M.F., 2009. In vitro metabolism of pyrethroid pesticides by rat and human hepatic microsomes and cytochrome P450 isoforms. Drug Metab. Dispos. 37, 221–228. https://doi.org/10.1124/dmd.108.022343.

Shirasaka, Y., Kawasaki, M., Sakane, T., Omatsu, H., Moriya, Y., Nakamura, T., Sakaeda, T., Okumura, K., Langguth, P., Yamashita, S., 2006. Induction of human P-glycoprotein in Caco-2 cells: development of a highly sensitive assay system for P-glycoprotein-mediated drug transport. Drug Metab. Pharmacokinet. 21, 414–423. https://doi.org/10.2133/dmpk.21.414.

Singh, A.K., Saxena, P.N., Sharma, H.N., 2009. Stress induced by beta-cyfluthrin, a type-2 pyrethroid, on brain biochemistry of Albino rat (Rattus norvegicus). Biol. Med. 1, 74–86. https://doi.org/10.4172/0974-8369.1000018.

Syed, F., Chandravanshi, L.P., Khanna, V.K., Soni, I., 2016. Beta-cyfluthrin induced neurobehavioral impairments in adult rats. Chem. Biol. Interact. 243, 19–28. https://doi.org/10.1016/j.cbi.2015.11.015.

Timchalk, C., Nolan, R.J., Mendrala, A.L., Dittenber, D.A., Brzak, K.A., Mattsson, J.L., 2002. A physiologically based pharmacokinetic and pharmacodynamic (PBPK/PD) model for the organophosphate insecticide chlorpyrifos in rats and humans. Toxicol. Sci. 66, 34–53. https://doi.org/10.1093/toxsci/66.1.34.

Tornero-Velez, R., Davis, J., Scollon, E.J., Starr, J.M., Setzer, R.W., Goldsmith, M.-R., Chang, D.T., Xue, J., Zartarian, V., De Vito, M.J., et al., 2012. A pharmacokinetic model of cis- and trans-permethrin disposition in rats and humans with aggregate exposure application. Toxicol. Sci. 130, 33–47. https://doi.org/10.1093/toxsci/kfs236.

Weber, C.R., 2012. Dynamic properties of the tight junction barrier. Ann. N. Y. Acad. Sci. 1257, 77–84. https://doi.org/10.1111/j.1749-6632.2012.06528.x.

Weksler, B., Romero, I.A., Couraud, P.O., 2013a. The HCMEC/D3 cell line as a model of the human blood brain barrier. Fluids Barriers CNS 10, 16. https://doi.org/10.1186/2045-8118-10-16.

Weksler, B., Romero, I.A., Couraud, P.O., 2013b. The HCMEC/D3 cell line as a model of the human blood brain barrier. Fluids Barriers CNS 10, 16. https://doi.org/10.1186/2045-8118-10-16.

Whitney, K.D., Seidler, F.J., Slotkin, T.A., 1995. Developmental neurotoxicity of chlorpyrifos: cellular mechanisms. Toxicol. Appl. Pharmacol. 134, 53–62. https://doi.org/10.1006/taap.1995.1168.

Wilhelm, I., Krizbai, I.A., 2014. In vitro models of the blood–brain barrier for the study of drug delivery to the brain. Mol. Pharm. 11, 1949–1963. https://doi.org/10.1021/mp500046f.

Yang, J., Mutkus, L.A., Sumner, D., Stevens, J.T., Eldridge, J.C., Strandhoy, J.W., Aschner, M., 2001a. Transendothelial permeability of chlorpyrifos in RBE4 monolayers is modulated by astrocyte-conditioned medium. Mol. Brain Res. 97, 43–50. https://doi.org/10.1016/S0169-328X(01)00296-0.

Yang, J., Mutkus, L.A., Sumner, D., Stevens, J.T., Eldridge, J.C., Strandhoy, J.W., Aschner, M., 2001b. Transendothelial permeability of chlorpyrifos in RBE4 monolayers is modulated by astrocyte-conditioned medium. Mol. Brain Res. 97, 43–50. https://doi.org/10.1016/S0169-328X(01)00296-0.

Yuan, S., Liu, K., Qi, Z., 2020. Occludin regulation of blood–brain barrier and potential therapeutic target in Ischemic stroke. Brain Circ. 6, 152. https://doi.org/10.4103/bc.bc_29_20.